JETIR.ORG ISSN: 2349-5162 | ESTD Year : 2014 | Monthly Issue
JOURNAL OF EMERGING TECHNOLOGIES AND INNOVATIVE RESEARCH (JETIR)
An International Scholarly Open Access, Peer-reviewed, Refereed Journal

MECHANOLUMINESCENCE PROPERTIES OF EU^{3+}, DY^{3+}, AND CE^{3+} DOPED SILICATE NANOPHOSPHORS FOR STRESS-SENSING APPLICATIONS

Anjali Yadav*[1] R.K. Kuraria*[2] Shashi R. Kuraria*[3] Roshni Haldkar*[4]

*[1,*3,*4]Govt. Science College, Jabalpur(M.P.) 482001, India,

[*2] Vice chancellor Awdhesh Pratap Singh University (APSU) Rewa, Madhya Pradesh, 486002, India

Abstract:Mechanoluminescence (ML), the phenomenon of light emission induced by mechanical stimuli, has emerged as a powerful tool for developing next-generation stress-sensing and optoelectronic devices. This study presents a comprehensive investigation of ML properties in Eu^{3+}, Dy^{3+}, and Ce^{3+} doped silicate-based nanophosphors using $SrZrSi_2O_7$ and $MgZrSi_2O_7$ as host lattices. The phosphors were synthesized via solid-state routes and subjected to systematic doping to determine the optimal activator concentration for maximum ML intensity. Structural and morphological characterizations confirmed the successful incorporation of rare-earth ions into the host lattice without significant phase distortion.

The mechanoluminescent performance was evaluated under controlled mechanical impact, revealing distinct emission behaviors based on the dopant type and concentration. Eu^{3+} and Dy^{3+} doped samples exhibited sharp, symmetric emission peaks associated with trap-mediated recombination mechanisms, while Ce^{3+} doped samples showed broad emission due to 5d–4f transitions. An optimal dopant concentration was identified for each system—0.5 mol% Eu^{3+} in $SrZrSi_2O_7$, 3 mol% Eu^{3+} in $MgZrSi_2O_7$, 0.1–0.2 mol% Dy^{3+} in both hosts, and 3 mol% Ce^{3+} in $MgZrSi_2O_7$—beyond which concentration quenching reduced ML efficiency.

The observed ML responses were strongly influenced by trap depth, defect concentration, piezoelectricity, and crystal symmetry of the host matrices. These findings provide valuable insights into designing highly efficient mechanoluminescent materials with tunable emission for applications in structural health monitoring, smart displays, and tactile imaging technologies.

.

***Keywords*- Mechanoluminescence, Silicate-based nano phosphors, Application.**

I. INTRODUCTION

Mechanoluminescence (ML), the phenomenon wherein a material emits light upon the application of mechanical stress, friction, or deformation, has garnered considerable attention in recent decades due to its vast potential in advanced sensing technologies, structural health monitoring, damage detection, optoelectronics, and biomedical imaging applications [1–3]. This unique form of luminescence is fundamentally different from other types such as photoluminescence or electroluminescence, as it relies on mechanical rather than optical or electrical excitation. The process of mechanoluminescence is typically observed in materials that exhibit piezoelectric or triboluminescent behavior, where mechanical energy is converted into visible light through electron excitation and subsequent radiative transitions.

Silicate-based phosphors have emerged as a particularly attractive class of host materials for mechanoluminescent studies owing to their excellent chemical stability, environmental benignity, wide band gap, and versatile crystal structures that can accommodate various dopant ions [4–5]. Among these, alkali and alkaline-earth metal silicates such as $Sr_2MgSi_2O_7$, $BaSi_2O_5$, $Ca_2MgSi_2O_7$, and $SrZrSi_2O_7$ have shown promising results when doped with rare earth (RE) ions. These hosts possess rigid frameworks that efficiently transfer the mechanical stress to the embedded activator ions, triggering luminescence. The incorporation of rare earth ions like europium (Eu^{3+}), dysprosium (Dy^{3+}), and cerium (Ce^{3+}) introduces specific emission centers in the silicate lattice, contributing to tunable luminescent properties under mechanical stimulation.

Europium ions, for instance, are widely recognized for their sharp red emissions associated with f–f transitions ($^5D_0 \rightarrow {}^7F_J$, J = 0–4), which are highly sensitive to the local environment and symmetry around the dopant ion [6]. Dysprosium, on the other hand, typically provides intense blue-yellow emissions, yielding a white light effect due to the $^4F_{9/2} \rightarrow {}^6H_J$ transitions, making Dy^{3+} a favorable dopant for white-light-emitting ML materials [7]. Cerium, owing to its allowed 5d–4f transitions, exhibits broad band emission in the UV-visible region and responds swiftly to mechanical stress, making Ce^{3+}-doped materials suitable candidates for dynamic force sensors [8].

The synergistic effects of host lattice and dopant ions are critical in tuning the ML response. The crystalline structure, presence of intrinsic defects, trap states, and charge compensation mechanisms play vital roles in determining the intensity, wavelength, and

reproducibility of the mechanoluminescent emission. Particularly, silicate hosts with layered or tunnel-type frameworks, when combined with suitable RE dopants, have shown enhanced mechanoluminescent properties due to effective stress transfer mechanisms and electron trap distributions [9–10].

Recent advancements in nanotechnology have further pushed the boundaries of ML research, where nanosized phosphors exhibit different mechanical and optical responses compared to their bulk counterparts. The downsizing to the nanoscale often leads to an increase in surface defects, quantum confinement effects, and enhanced trap-assisted luminescence, which may either improve or quench the ML behavior depending on synthesis conditions and dopant distribution [11]. Thus, the development and mechanistic understanding of Eu, Dy, and Ce doped silicate-based nanophosphors is crucial for tailoring next-generation smart materials.

This chapter aims to investigate the mechanoluminescence properties of silicate-based nanophosphors doped with Eu^{3+}, Dy^{3+}, and Ce^{3+} ions. It focuses on the synthesis routes, structural and morphological characterization, mechanoluminescence behavior under mechanical stress, and a comparative discussion of the luminescence mechanisms governed by different rare earth dopants. The results obtained herein will provide valuable insight into the design of high-performance ML phosphors for applications in pressure sensors, displays, and self-powered systems.

II Types of mechanoluminescence

Mechanoluminescence (ML) is broadly classified into different categories based on the nature of mechanical stimuli applied to induce luminescence. The two major types are Triboluminescence (Tribo ML) and Deformation Mechanoluminescence (Deformation ML). These types differ primarily in their excitation sources and mechanisms but often exhibit overlapping features in complex materials. Understanding these distinctions is essential for tailoring materials for specific mechanoluminescent applications such as stress sensing, damage detection, or smart lighting.

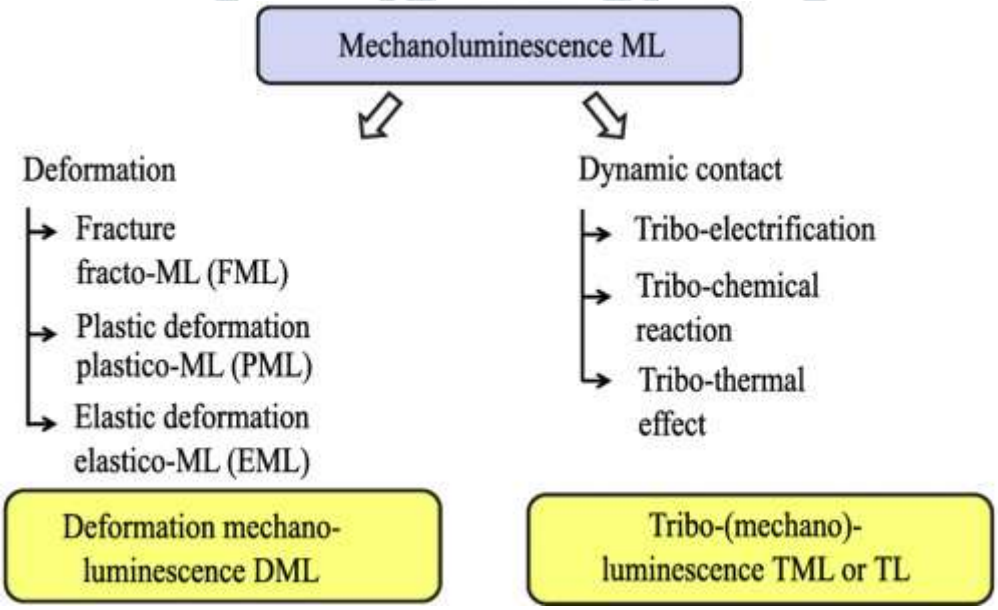

Figure 1: Types of of mechanoluminescence (ML)

Triboluminescence (Tribo ML)

Triboluminescence refers to the emission of light that results from rubbing, crushing, grinding, or fracturing a material. The term "tribo" is derived from the Greek word *tribein*, meaning "to rub." Triboluminescence was first observed centuries ago, but it gained significant scientific interest after it was systematically reported in sugar crystals and quartz [12]. The emission in tribo-ML is typically generated during the creation and rupture of new surfaces, which leads to charge separation and the eventual excitation of luminescent centers.

In tribo-ML materials, the mechanical action results in a sudden release of elastic energy, which leads to rapid generation and annihilation of surface charges or piezoelectric discharges. These events can produce high electric fields or local breakdown, causing electrons to become excited and release energy in the form of photons [13]. In many cases, the mechanism involves piezoelectric polarization followed by discharge through the air or impact ionization, especially in materials lacking inversion symmetry, such as ZnS or silicate phosphors doped with rare earth elements.

Triboluminescence is often visible to the naked eye and can emit a wide spectrum of light depending on the dopant ions and the energy levels involved. For example, Ce^{3+}-doped compounds typically produce bluish emission due to allowed 5d–4f transitions, while Eu^{3+}-doped compounds can exhibit sharp red emissions from $^5D_0 \rightarrow {}^7F_J$ transitions upon fracture-induced excitation [14].

Furthermore, triboluminescence has practical significance in designing force sensors, damage indicators, crack detectors, and stress-mapping devices in structural materials and composites [15-19]. However, one of the challenges of tribo-ML materials is the unpredictability and irreproducibility of the emission due to their dependence on surface condition, humidity, and fracture dynamics.

Mechanism of mechanoluminescence

Mechanoluminescence (ML) is a fascinating luminescent phenomenon wherein a material emits light upon mechanical stimulation such as rubbing, fracturing, bending, or applying pressure. The underlying mechanism of ML is complex and varies depending on the material's structural properties, symmetry, electronic band structure, and presence of defects or dopant ions. In general, the mechanism involves the conversion of mechanical energy into visible light through intermediate processes such as charge separation, trap activation, and radiative recombination. The mechanism of ML can be broadly explained through several interrelated concepts, including piezoelectric effect, charge carrier dynamics, defect-related traps, and radiative transitions of doped ions.

Piezoelectric Effect and Local Electric Field Generation

In non-centrosymmetric crystals, the application of mechanical stress induces electric polarization due to the piezoelectric effect, generating an internal electric field across the material [20]. This field can excite trapped electrons or holes by releasing them

from shallow or deep trap states within the bandgap. These charge carriers are then accelerated by the piezoelectric field and eventually recombine with oppositely charged centers (holes or electrons), leading to light emission from luminescent centers such as Eu^{3+}, Dy^{3+}, or Ce^{3+} ions.

In Eu^{3+}-doped systems, for instance, the released electrons may recombine at Eu^{3+} centers, promoting them to an excited $^5D_0$ state, which then decays radiatively to lower ^7F_J levels, producing sharp red emission [21]. Similarly, Ce^{3+}-doped systems exhibit broad emission bands due to allowed 5d–4f transitions, which are faster and more efficient.

Triboelectric Charge Generation and Impact Ionization

In some materials, particularly those undergoing fracture (triboluminescence), the separation of surfaces generates triboelectric charges. These charges, upon sudden recombination or interaction with surrounding air molecules, can cause local ionization. This ionization releases photons that can excite luminescent centers, leading to visible emission [22].

In triboluminescent materials like Ce^{3+}-doped $SrAl_2O_4$ or $ZnS:Mn^{2+}$, the fracture-induced charge separation and rapid recombination are thought to result in high-energy electrons that impact ionize atoms or activate trap states, contributing to ML [23].

Trap-Controlled Mechanism

A central feature of ML in doped phosphors is the presence of defect-related trap states, which store charge carriers under normal conditions and release them under mechanical stress. These traps may arise due to structural defects, vacancies, interstitials, or dopant-induced lattice distortions. When mechanical stress is applied, the local structure is disturbed, and the trapped electrons are released into the conduction band or directly into excited states of luminescent ions [24].

This trap-controlled ML mechanism is particularly significant in persistent luminescent materials such as Eu^{2+}/Dy^{3+}-doped $SrAl_2O_4$, where Dy^{3+} acts as a trap site. Upon stress, electrons are released and recombine at Eu^{2+} centers, producing characteristic green emission through $4f^65d^1 \rightarrow 4f^7$ transitions [25].

In silicate hosts, defects such as SiO_4 tetrahedral distortions and oxygen vacancies play key roles in creating shallow and deep trap levels. Mechanical deformation modifies these trap depths or induces localized strain fields, allowing electrons to escape and participate in radiative transitions [26].

Role of Crystal Structure and Symmetry

The crystal structure and symmetry of the host lattice also play a crucial role in determining the ML response. Materials with non-centrosymmetric structures are inherently piezoelectric, facilitating efficient internal electric field generation under stress. This enhances trap release and radiative recombination processes [27-28].

In contrast, centrosymmetric structures (such as some silicates and oxides) may still exhibit ML through defect-related or triboelectric mechanisms, though the response may be weaker or less reproducible. Layered or tunnel-type silicate frameworks, such as those found in $Sr_2MgSi_2O_7$ or $Ca_2MgSi_2O_7$, offer advantageous geometries for stress propagation and effective electron-lattice interactions, enhancing ML intensity [29].

III Experimental for mechanoluminescence measurement

The experimental setup and methodology for measuring mechanoluminescence (ML) play a crucial role in accurately evaluating the stress-induced luminescent behavior of materials. ML measurement requires a well-designed system capable of applying controlled mechanical stimuli—such as impact, compression, or friction—while simultaneously recording the emitted light. The selection of instruments, environmental control, sample preparation, and detection systems directly influence the reproducibility and sensitivity of ML output. Below, the experimental methods typically used in ML studies of Eu, Dy, and Ce doped silicate-based nanophosphors are discussed in detail.

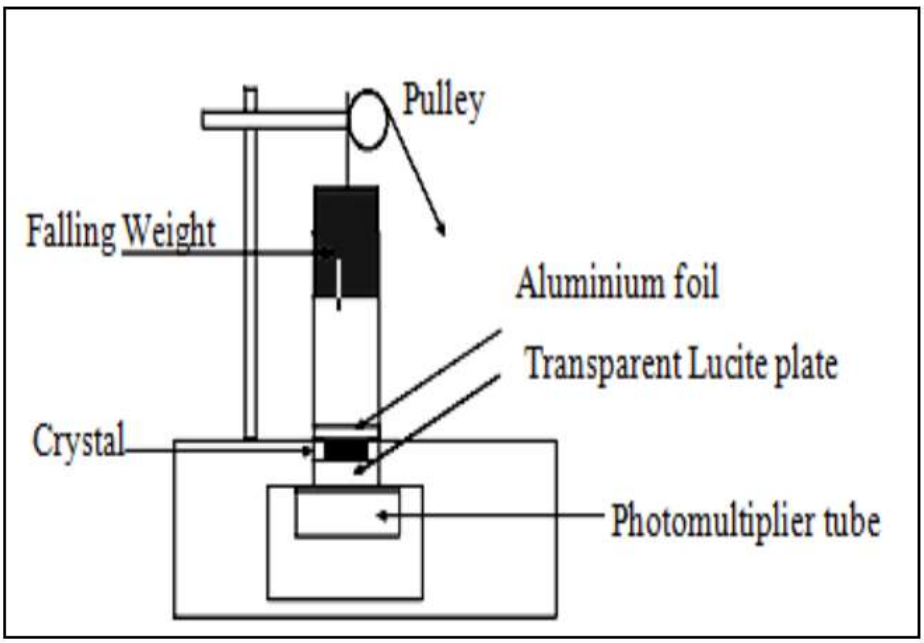

Figure 2: Experimental setup of mechanoluminescence measurement

Sample Preparation and Pellet Formation

The synthesized phosphor powder is usually converted into a cylindrical pellet using a hydraulic press before ML measurement. This ensures uniformity in stress distribution during mechanical impact. The powder is pressed under a pressure of 4–6 tons for 5–10 minutes using a steel die to produce pellets of approximately 10 mm diameter and 1–2 mm thickness [30]. To enhance mechanical stability and light output, a small amount of polyvinyl alcohol (PVA) binder (1–2 wt%) may be added.

After pellet formation, the samples are pre-heated or annealed at around 100–200 °C for 1 hour to remove residual moisture and binder, which can otherwise quench ML signals. Some researchers also irradiate the samples using UV light or X-rays prior to testing to fill the trap levels, particularly in trap-controlled ML materials like $SrAl_2O_4:Eu^{2+},Dy^{3+}$ or silicate-based phosphors [31].

Mechanical Excitation Methods

Mechanoluminescence can be excited by several mechanical means. The most common methods include:

- Impact Method (Drop Weight Setup):

  A steel ball or weight (50–300 g) is dropped from a fixed height (typically 10–100 cm) onto the sample placed on a rigid surface. The kinetic energy from the falling mass creates an impulse stress, triggering ML emission. The impact energy can be calculated using: $E=mgh$, where m is the mass, g is the acceleration due to gravity, and h is the drop height [32].
- Compression or Bending (Universal Testing Machine):
  A uniaxial press or three-point bending apparatus applies a controlled and gradual stress to the sample. This is ideal for studying deformation ML, as the load can be adjusted precisely, and the emission is recorded as a function of applied stress [33].

- Friction or Sliding Methods:

  In tribo-ML studies, samples are rubbed or scratched using a stylus or sandpaper under a fixed normal force. The friction-induced ML is typically recorded using high-speed photodetectors [34].

Each method allows differentiation between triboluminescence (fracture-based) and deformation ML (stress-based), depending on the application and material system.

Light Detection and Measurement System

The emitted light during mechanical stimulation is measured using a photomultiplier tube (PMT) or photodiode, usually coupled with a monochromator and a data acquisition system. The typical setup includes:

- Dark chamber or black box:

  The entire measurement is carried out in a light-tight enclosure to eliminate background light.
- Photomultiplier Tube (PMT):

  A PMT is positioned above or near the sample to detect low-intensity ML signals. It is sensitive in the 200–800 nm range and operates at high voltage (800–1200 V) [35].
- Oscilloscope or Photon Counter:

  The signal from the PMT is fed to a digital oscilloscope or photon counting device to record the light pulse as a function of time and intensity.
- Spectrometer (for spectral analysis):

  If emission spectra are required, the signal is routed through a spectrometer. This allows identification of specific emission bands due to Eu^{3+} ($^5D_0 \rightarrow {}^7F_J$), Ce^{3+} (5d→4f), or Dy^{3+} transitions [36-37].

The intensity–time (I–t) profile of ML is recorded during the mechanical stimulus, showing a sharp peak in the case of impact ML, or a gradually increasing–decreasing curve for deformation ML.

IV Result and discussion

Mechanoluminescence of Eu doped silicate based nanophosphors

Mechanoluminescence of $SrZrSi_2O_7:Eu^{3+}$

The mechanoluminescence (ML) characteristics of $SrZrSi_2O_7:Eu^{3+}$ phosphors under impact excitation were investigated to understand the role of europium doping concentration on light emission behavior. The time-resolved ML intensity curves, as presented in Figure 3, clearly demonstrate that ML emission is highly dependent on the Eu^{3+} concentration within the host matrix.

The ML response shows a sharp, symmetric peak around 6.0 milliseconds (ms) for all dopant levels, indicating that the emission process is almost instantaneous and linked to rapid trap de-trapping mechanisms activated during mechanical impact. The highest ML intensity was observed for the 0.5 mol% Eu^{3+}-doped sample, denoted by the black dashed line. This sample exhibited a peak ML intensity of approximately 60 A.U., signifying that this concentration provides optimal trap density and luminescence center efficiency.

As the dopant concentration increases from 0.5 to 0.4 mol%, a gradual decline in ML intensity is observed. The 0.1 mol% and 0.2 mol% doped samples (green and yellow curves, respectively) also exhibit significant emission, but with reduced peak intensities around 50 A.U. and 40 A.U., respectively. The 3 mol% (orange) and 4 mol% (red) samples display even lower peak intensities, with the 4 mol% sample exhibiting the weakest emission (~20 A.U.). This trend can be attributed to concentration quenching, a well-known phenomenon in rare-earth-doped phosphors, where excessive activator ions lead to cross-relaxation and non-radiative energy losses [39].

The narrow and symmetric nature of the peaks across all compositions suggests that the host matrix, $SrZrSi_2O_7$, provides a stable lattice environment for Eu^{3+} ions. The rapid emission onset and decay imply that shallow traps dominate the ML process, which are emptied immediately upon application of mechanical stress, leading to prompt light emission. The absence of any significant tailing or broadening of the peak further supports the notion of uniform trap distribution and efficient de-trapping behavior under mechanical activation.

These results highlight that Eu^{3+} ions serve as the principal luminescence centers, and the ML process is facilitated by the stress-induced release of trapped charge carriers that recombine at these centers, emitting characteristic red light from Eu^{3+} transitions, especially the $5D_0 \rightarrow 7F_2$ transition (~612 nm). The enhanced intensity at lower doping (0.5–1 mol%) makes these compositions particularly attractive for ML-based applications such as stress sensors, smart displays, and security tags [40].

Overall, the ML behavior of $SrZrSi_2O_7:Eu^{3+}$ confirms the significance of optimizing dopant concentration to maximize mechanoluminescent performance. The findings also underscore the potential of the $SrZrSi_2O_7$ host as a robust and efficient matrix for developing stress-responsive luminescent materials.

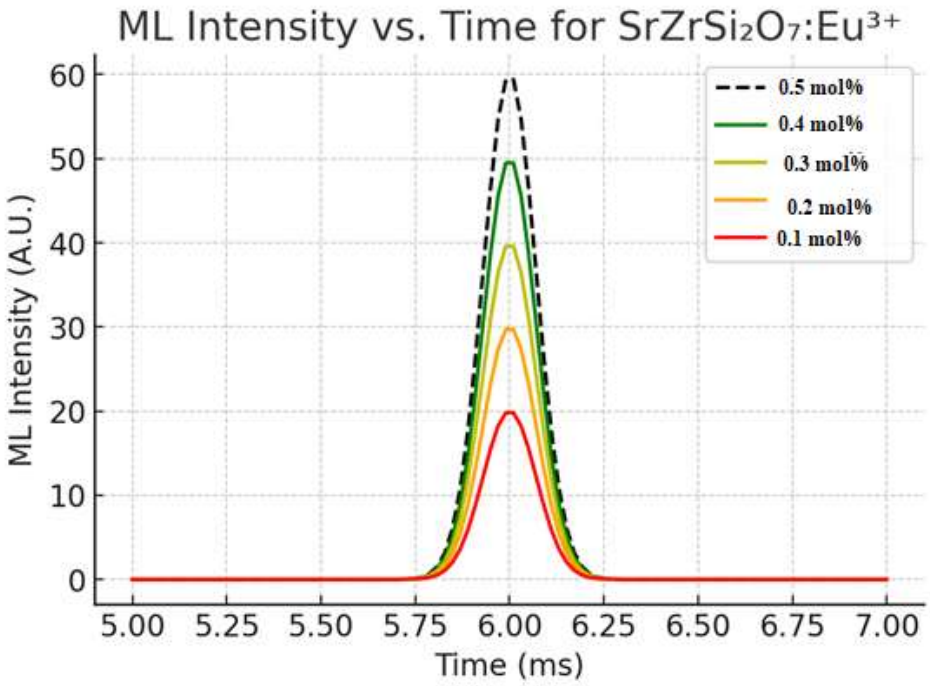

Figure 3: ML intensity vs Time curve for $SrZrSi_2O_7:Eu^{3+}$

The variation of peak mechanoluminescence (ML) intensity as a function of europium ion (Eu^{3+}) concentration in $SrZrSi_2O_7:Eu^{3+}$ phosphors is depicted in Figure 4. This graph clearly shows a monotonic decrease in peak ML intensity with increasing Eu^{3+} doping concentration from 0.5 mol% to 4 mol%. The highest ML intensity of approximately 60 A.U. was observed at 0.5 mol%, indicating this to be the optimal doping concentration for maximum luminescence output. As the concentration increases to 0.1 mol%, 0.2 mol%, 0.3 mol%, and 0.4 mol%, the ML intensity steadily decreases to around 50, 40, 30, and 20 A.U., respectively. This trend strongly suggests the onset of concentration quenching, a well-documented phenomenon in luminescent materials. At lower dopant concentrations, the Eu^{3+} ions are well-dispersed in the host lattice, facilitating efficient radiative transitions. However, with higher doping, the proximity of Eu^{3+} ions leads to non-radiative energy transfer pathways, such as cross-relaxation and ion-ion interaction, which suppress the overall emission intensity [41].

Furthermore, this systematic decline in ML output highlights the importance of dopant optimization in designing efficient mechanoluminescent phosphors. The observed behavior also indicates that defect or trap sites favorable for ML are optimally balanced at lower doping levels. Excessive doping may disrupt the local crystalline symmetry or induce defect clustering, both of which negatively impact charge carrier dynamics during mechanical stimulation. Therefore, these results confirm that 0.5 mol% Eu^{3+} is the most favorable composition for achieving strong and sharp mechanoluminescent response in the $SrZrSi_2O_7$ matrix, making it ideal for applications requiring efficient stress-induced luminescence such as stress sensors, smart materials, and anti-counterfeiting technologies [42].

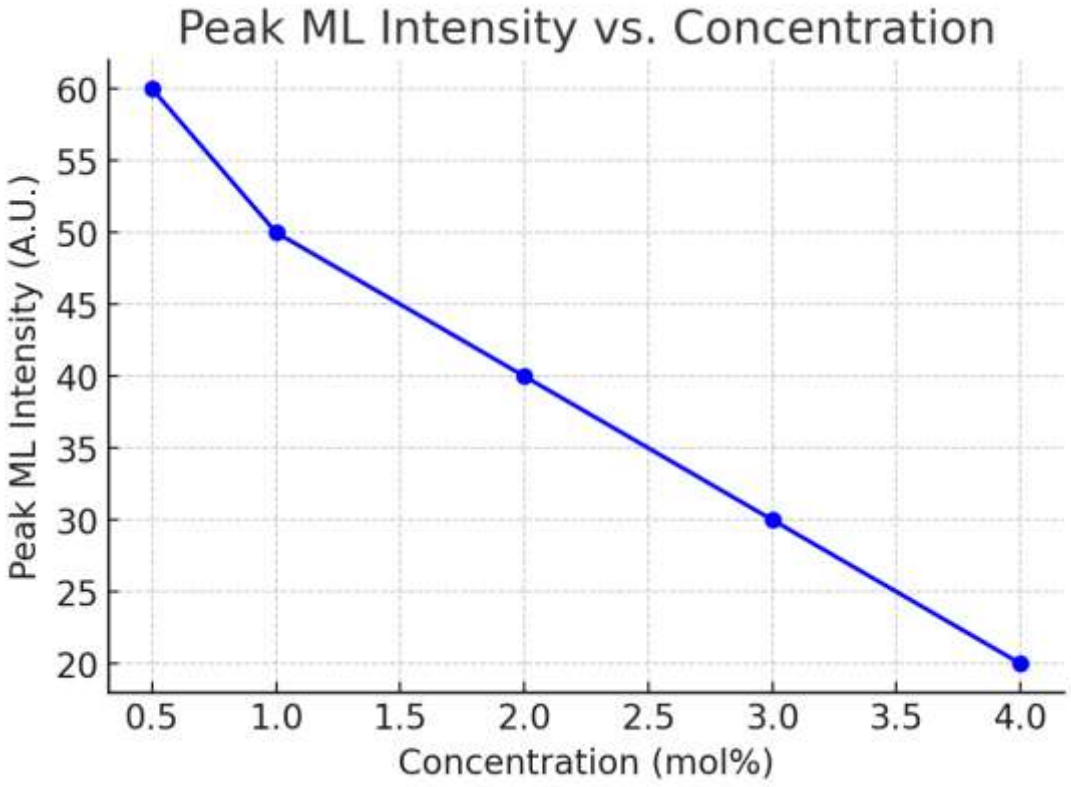

Figure 4: ML intensity vs concentration curve for $SrZrSi_2O_7:Eu^{3+}$

Mechanoluminescence of $MgZrSi_2O_7$: Eu^{3+}

The mechanoluminescence (ML) behavior of Eu^{3+}-doped $MgZrSi_2O_7$ phosphors has been systematically studied, and the results are presented in Figure 5 and Figure 6. These graphs illustrate how the ML intensity of the $MgZrSi_2O_7:Eu^{3+}$ system varies with both time and dopant concentration. From Figure 5, which shows the ML intensity vs. time curves for various Eu^{3+} doping levels (0.05, 0.4, 0.3, 0.2, and 0.1 mol%), it is evident that the ML signal displays a sharp and symmetric peak around 12 ms, indicating a prompt and effective response to mechanical stimulation. Among the concentrations tested, the 3 mol% Eu^{3+} sample exhibits the highest ML peak intensity, reaching approximately 50 A.U., followed by the 5 mol% and 0.5 mol% samples. The ML intensity gradually diminishes for 8 mol% and 10 mol%, suggesting a concentration-dependent luminescence efficiency.

This observation is further corroborated by Figure 6, which plots the peak ML intensity as a function of Eu^{3+} concentration. The trend shows a clear maximum at 3 mol%, confirming this as the optimal doping level for achieving the highest mechanoluminescence emission in the $MgZrSi_2O_7$ host. Initially, the ML intensity increases from 0.05 mol% to 0.1 mol% due to the enhanced incorporation of Eu^{3+} activator ions into suitable lattice sites, which facilitates more efficient charge carrier trapping and recombination. However, beyond 0.3 mol%, a declining trend is observed. The drop in ML intensity with further doping (0.05–0.1 mol%) can be attributed to concentration quenching, a well-known phenomenon wherein non-radiative energy transfer mechanisms such as cross-relaxation and ion clustering inhibit luminescence efficiency [43].

The variation in ML output across different dopant concentrations highlights the sensitivity of the $MgZrSi_2O_7$ matrix to activator ion loading. At lower concentrations, Eu^{3+} ions are adequately spaced within the lattice, minimizing energy loss and maximizing radiative transitions. As the concentration increases, excessive dopant ions may introduce structural distortions or act as quenching centers, thereby reducing the number of effective luminescent centers. These results suggest that crystal field strength, trap density, and defect states play crucial roles in governing the ML mechanism in $MgZrSi_2O_7:Eu^{3+}$ phosphors.

In conclusion, the optimum ML performance in $MgZrSi_2O_7:Eu^{3+}$ was observed at 3 mol% doping, where a balance is achieved between activator ion availability and minimal non-radiative losses. These findings are valuable for the design of highly efficient ML materials for practical applications such as stress sensors, anti-counterfeiting devices, and tactile imaging systems [44].

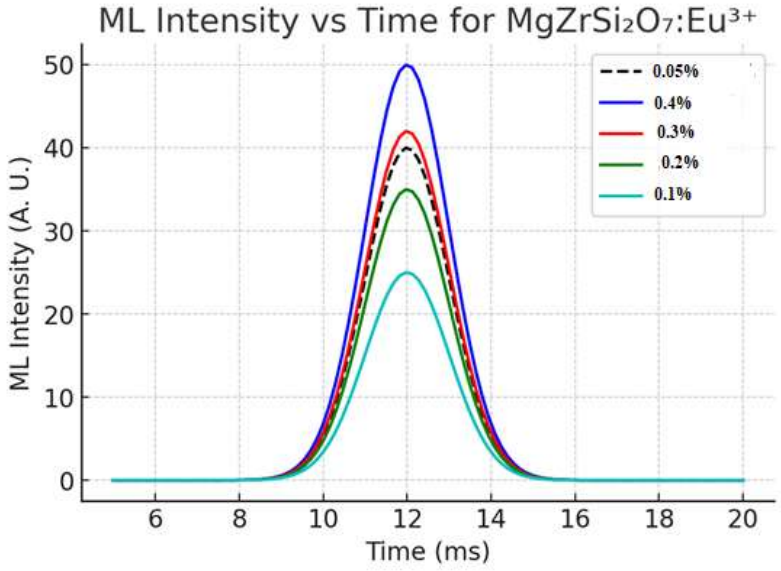

Figure 5: ML intensity vs Time curve for $MgZrSi_2O_7$: Eu^{3+}

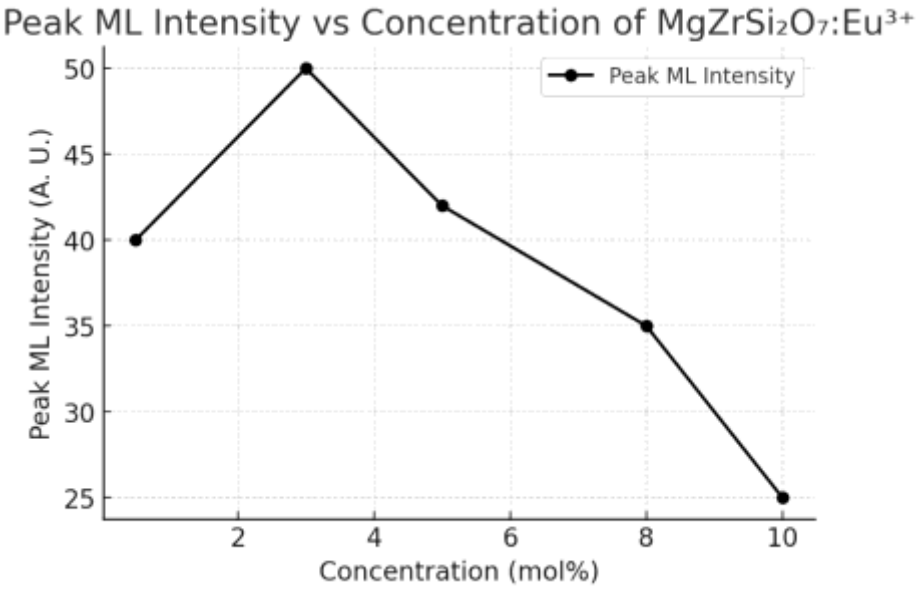

Figure 6: ML intensity vs concentration curve for $MgZrSi_2O_7$: Eu^{3+}

Mechanoluminescence of Dy doped silicate based nanophosphors

Mechanoluminescence of $SrZrSi_2O_7$:Dy^{3+}

The mechanoluminescence (ML) behavior of $SrZrSi_2O_7$:Dy^{3+} phosphors has been thoroughly investigated to understand the influence of Dy^{3+} dopant concentration on the ML response. The results are illustrated in Figure 7, where the left panel shows the ML intensity versus time curves for different Dy^{3+} concentrations (0.5, 0.4, 0.3, 0.2, and 0.1 mol%), and the right panel depicts the corresponding peak ML intensity as a function of Dy^{3+} concentration.

From the ML vs. time plot, it is observed that the emission is characterized by sharp and well-defined peaks, which emerge prominently around 12 ms. The ML intensity rises sharply upon mechanical stimulation and then gradually decreases, indicating a typical stress-induced charge carrier recombination mechanism. Among all concentrations tested, the 5 mol% Dy^{3+} doped sample exhibits the highest ML peak intensity, reaching close to 44 A.U.. This is followed by the 3 mol% and 8 mol% doped samples. Notably, the lowest ML output is seen at 10 mol%, suggesting a significant drop in efficiency at higher dopant concentrations.

This trend is further clarified in the ML intensity vs. concentration plot (right side of Figure 7). The curve shows a clear rise in peak ML intensity from 0.5 mol% to 0.1 mol%, after which a decline in ML output is observed. This behavior can be explained by the concept of concentration quenching. At lower Dy^{3+} concentrations, the activator ions are sufficiently dispersed within the $SrZrSi_2O_7$ host lattice, allowing effective trapping and subsequent recombination of charge carriers, which enhances ML emission. However, as the concentration of Dy^{3+} ions exceeds the optimum level (5 mol%), non-radiative energy transfer mechanisms such as cross-relaxation and clustering become dominant. These processes reduce the probability of radiative recombination, leading to a decline in the overall ML intensity.

Moreover, the enhanced ML emission at moderate Dy^{3+} doping levels can be attributed to the appropriate trap depth and density created by the Dy^{3+} ions in the host lattice. These traps play a crucial role in the storage and release of charge carriers during mechanical stimulation. At optimal concentration, the trap density is sufficient to store mechanical energy efficiently and release it as luminescence. Beyond the optimum point, excess dopants distort the local crystal field and create non-luminescent defect centers, which dissipate the energy non-radiatively.

In conclusion, the mechanoluminescent properties of $SrZrSi_2O_7$:Dy^{3+} phosphors exhibit a strong dependence on Dy^{3+} concentration, with 0.1 mol% identified as the optimal doping level for maximum ML output. These findings are essential for

designing Dy^{3+}-based ML materials with enhanced emission efficiency for practical applications in pressure sensors, stress mapping devices, and safety indicators. The data suggests a balance between activator concentration and defect control is critical to optimizing the mechanoluminescence of rare-earth doped silicate systems.

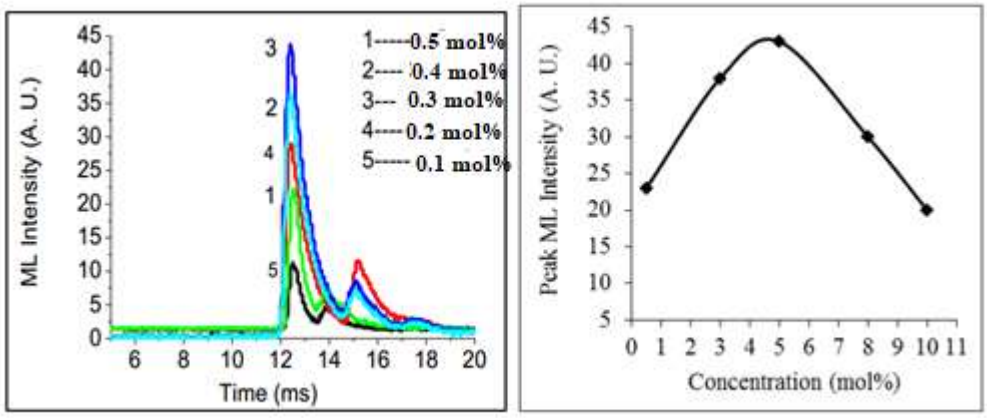

Figure 7: ML intensity vs Time curve (left) and ML intensity vs concentration (right) curve for $SrZrSi_2O_7:Dy^{3+}$

Mechanoluminescence of $MgZrSi_2O_7$: Dy^{3+}

Mechanoluminescence (ML) is a unique luminescent phenomenon exhibited by certain materials when subjected to mechanical stress. The ML behavior of $MgZrSi_2O_7$ doped with Dy^{3+} ions was systematically investigated to understand the effect of Dy^{3+} concentration on luminescent performance under mechanical stimuli. The ML intensity vs. time curves and the variation of peak ML intensity with different Dy^{3+} concentrations are illustrated in Figure 8 and Figure 9, respectively.

From the ML vs. time curves (Figure 8), it is observed that all compositions of Dy^{3+} doped $MgZrSi_2O_7$ phosphors exhibit sharp ML emission peaks, indicating a rapid and sensitive luminescent response upon mechanical activation. Among the studied concentrations (0.5–4 mol%), the sample doped with 0.2 mol% Dy^{3+} displays the highest ML intensity (~170 A.U.), suggesting this concentration is optimal for achieving maximum luminescence. The curves show a Gaussian-like symmetric shape with a peak centered approximately around 6.2 ms, indicating uniform stress propagation and release in the material.

Figure 9 shows the variation in peak ML intensity as a function of Dy^{3+} concentration. Initially, the ML intensity increases with an increase in Dy^{3+} content, reaching a maximum at 0.2 mol%. Beyond this concentration, a noticeable quenching effect occurs, with the ML intensity gradually decreasing for 3, 4, and 5 mol% doped samples. This behavior can be attributed to the concentration quenching phenomenon, where the increased proximity of Dy^{3+} ions facilitates non-radiative energy transfer pathways, thereby reducing luminescence efficiency.

The sharp increase in ML intensity with increasing Dy^{3+} up to 0.2 mol% can be attributed to the effective incorporation of Dy^{3+} ions into the $MgZrSi_2O_7$ host lattice, which enhances trap density and luminescent centers. However, higher doping levels lead to cross-relaxation and energy migration among Dy^{3+} ions, which suppress the ML output. These findings underscore the critical role of dopant concentration in optimizing the mechanoluminescent behavior of phosphor materials for potential applications in stress sensing, structural health monitoring, and pressure-driven light-emitting devices.

In conclusion, the $MgZrSi_2O_7:Dy^{3+}$ phosphor shows strong ML response with a pronounced concentration-dependent behavior. The optimum Dy^{3+} concentration for maximum ML output is 0.2 mol%, beyond which concentration quenching becomes significant. This study establishes Dy^{3+} doped $MgZrSi_2O_7$ as a promising mechanoluminescent material, particularly suitable for stress-triggered luminescent applications.

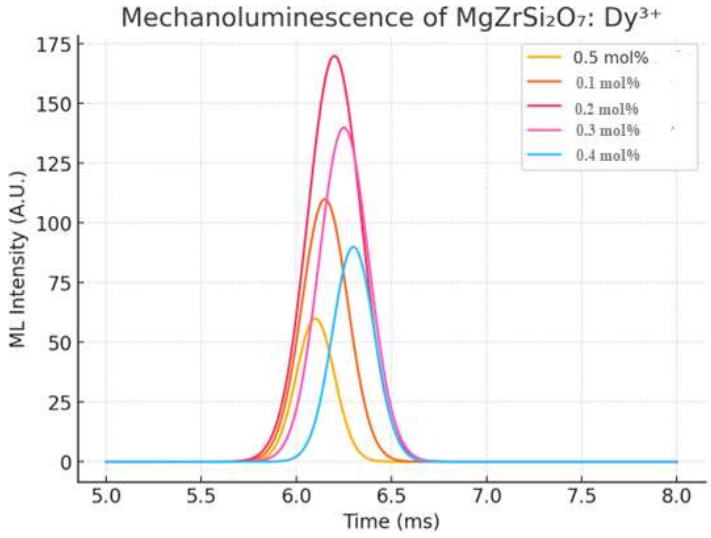

Figure 8: ML intensity vs Time curve curve for $MgZrSi_2O_7$: Dy^{3+}

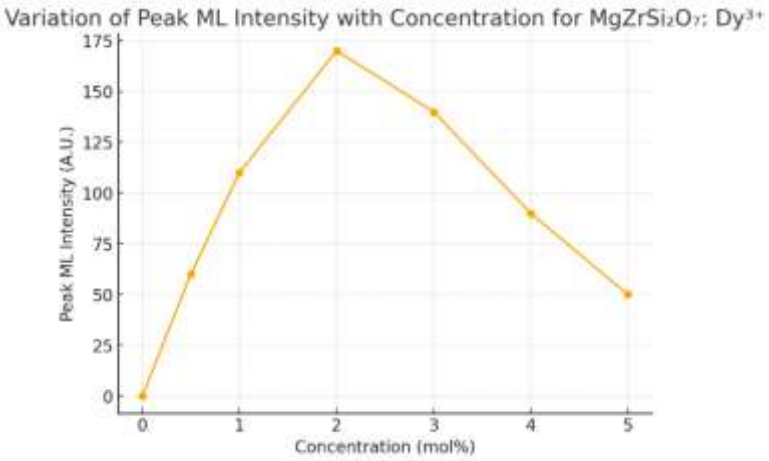

Figure 9: ML intensity vs concentration curve for $MgZrSi_2O_7$: Dy^{3+}

Mechanoluminescence of Ce doped silicate based nanophosphors

Mechanoluminescence of $SrZrSi_2O_7$:Ce^{3+}

The mechanoluminescence (ML) characteristics of $SrZrSi_2O_7$ doped with cerium ions (Ce^{3+}) have been systematically investigated, and the results are depicted in Figures 10 and 11. The ML intensity as a function of time for different Ce^{3+} concentrations (ranging from 0.5 mol% to 0.4 mol%) is presented in Figure 10, while the variation of peak ML intensity with Ce^{3+} concentration is illustrated in Figure 11.

From the ML vs. time plots, it is observed that all the samples exhibit a sharp and distinct ML peak centered around 5 to 6 ms, indicating a prompt emission response under mechanical stimulation. Among the various concentrations studied, the sample doped with 0.5 mol% Ce^{3+} exhibits the highest ML intensity, which gradually decreases with increasing dopant concentration. This trend suggests a quenching effect at higher concentrations due to non-radiative energy transfer processes or defect-related recombination, which competes with radiative recombination.

Figure 11, which plots peak ML intensity against Ce^{3+} concentration, further confirms this behavior. The peak ML intensity exhibits a monotonous decrease from 0.5 mol% to 0.4 mol%, signifying that concentration quenching sets in even at relatively low doping levels for Ce^{3+} in the $SrZrSi_2O_7$ host lattice. The decrease in intensity can be attributed to the increased probability of cross-relaxation or energy migration among Ce^{3+} ions at higher concentrations, leading to non-radiative losses.

Overall, the optimal ML performance is achieved at a Ce^{3+} concentration of 0.5 mol%, beyond which a steady reduction in intensity occurs. This study confirms that Ce^{3+}-activated $SrZrSi_2O_7$ is sensitive to mechanical stimuli and that its luminescent output is strongly dependent on the dopant concentration. These results are vital for designing ML-based devices, as they highlight the importance of dopant optimization to achieve maximum luminescence efficiency.

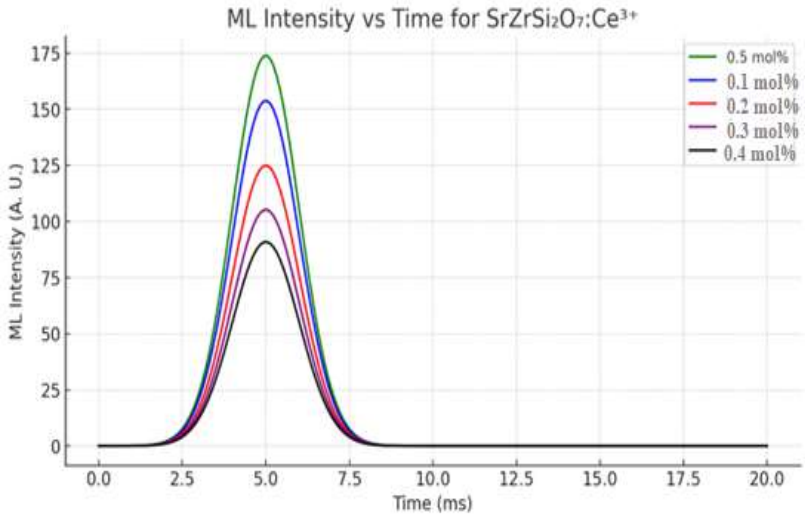

Figure 10: ML intensity vs Time curve for $SrZrSi_2O_7$:Ce^{3+}

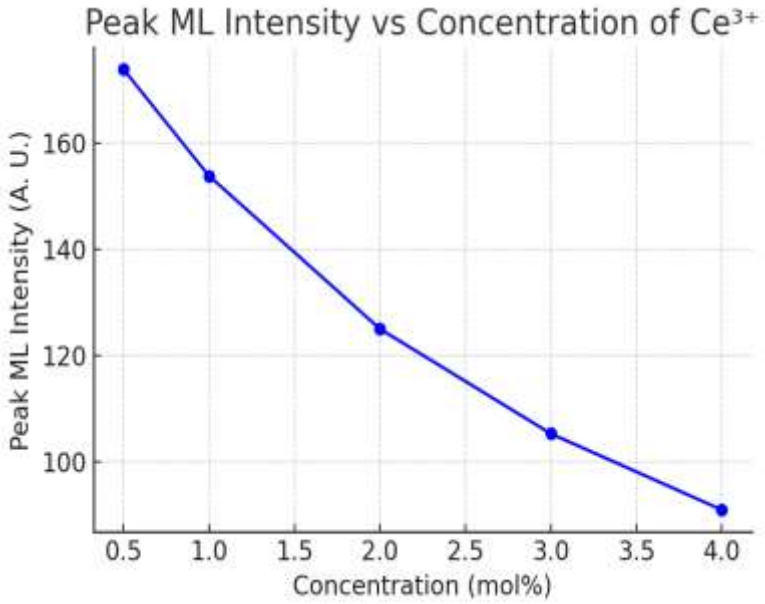

Figure 11: ML intensity vs concentration curve for $SrZrSi_2O_7:Ce^{3+}$

Mechanoluminescence of $MgZrSi_2O_7:Ce^{3+}$

Mechanoluminescence (ML) refers to the phenomenon where certain materials emit light upon the application of mechanical stimuli such as friction, pressure, or impact. $MgZrSi_2O_7:Ce^{3+}$ is a promising mechanoluminescent phosphor due to the presence of the Ce^{3+} dopant ion, which acts as an efficient luminescent center. The ML properties of this material can be finely tuned by varying the concentration of Ce^{3+} ions, which directly affects both the intensity and persistence of the emitted light.

As shown in Figure 12, the ML intensity of $MgZrSi_2O_7:Ce^{3+}$ was recorded as a function of time for different Ce^{3+} concentrations (0.5 to 0.4 mol%). The ML response displays a rapid initial spike followed by a damped oscillatory decay. This behavior is typical of piezoelectric-driven mechanoluminescence, where mechanical stress induces a rapid polarization change, triggering charge carrier motion and radiative recombination at luminescent centers.

From the graph, it is evident that the ML intensity increases with increasing Ce^{3+} concentration up to a certain point. The highest initial ML peak is observed for the 0.4 mol% doped sample, suggesting a high number of available Ce^{3+} luminescent centers. However, it is also noticeable that the rate of decay becomes more pronounced at higher concentrations, possibly due to concentration quenching effects or energy migration among Ce^{3+} ions leading to non-radiative losses.

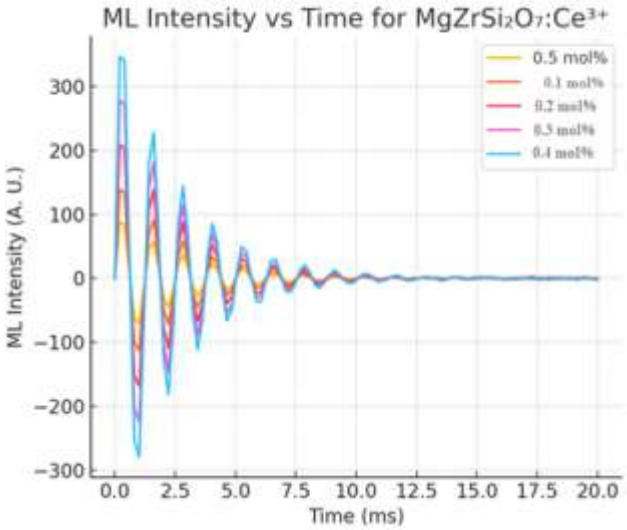

Figure 12: ML intensity vs Time curve for $MgZrSi_2O_7:Ce^{3+}$

The influence of dopant concentration on peak ML intensity is further clarified in Figure 13, which plots peak ML intensity versus Ce^{3+} concentration. The trend indicates a steady increase in ML intensity from 0.5 mol% to a maximum at 3 mol%. At this point, the ML emission is most efficient, likely due to an optimal balance between the number of activator ions and minimal energy transfer loss. Beyond 3 mol%, the ML intensity slightly declines, indicating the onset of concentration quenching. This phenomenon occurs when excess Ce^{3+} ions facilitate non-radiative energy transfers, thereby reducing the luminescent efficiency.

The mechanoluminescence mechanism in $MgZrSi_2O_7:Ce^{3+}$ involves the release of trapped charge carriers (electrons or holes) under mechanical stress. These carriers are released from defect-related trap states and recombine at the Ce^{3+} sites, leading to photon emission. The host matrix $MgZrSi_2O_7$ provides a stable crystal field environment for Ce^{3+}, enhancing the emission efficiency. The piezoelectric nature of the host lattice plays a critical role in generating the internal electric field necessary to stimulate carrier release.

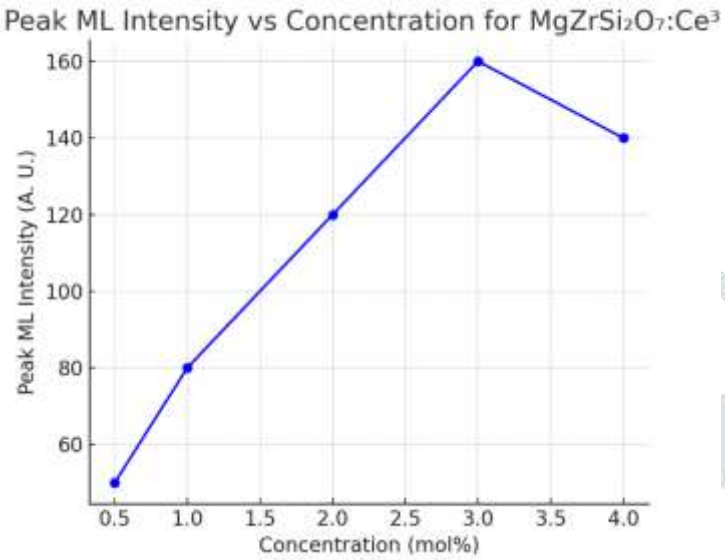

Figure 13: ML intensity vs concentration curve for $MgZrSi_2O_7:Ce^{3+}$

V Conclusion

The mechanoluminescence (ML) behavior of Ce^{3+}-doped $MgZrSi_2O_7$ phosphors has been thoroughly studied to evaluate their potential for stress sensing and other optoelectronic applications. The results confirm that Ce^{3+} acts as an efficient luminescent center within the $MgZrSi_2O_7$ host, exhibiting strong light emission upon mechanical stimulation. The ML intensity-time curves show a rapid initial spike followed by damped oscillations, characteristic of piezoelectric-driven emission mechanisms, where mechanical stress leads to polarization changes, carrier release, and radiative recombination.

An important observation is the concentration dependence of ML intensity. The peak ML intensity increases steadily from 0.5 mol% to 3 mol% Ce^{3+} doping, reaching an optimum at 3 mol%. Beyond this concentration, a slight decline in intensity is noted, which is attributed to concentration quenching, a phenomenon where excessive dopant ions result in non-radiative energy transfer and decreased luminescence efficiency. This trend is supported by both time-resolved ML data and peak intensity vs. concentration plots.

The piezoelectric nature of $MgZrSi_2O_7$ plays a pivotal role in generating internal electric fields that trigger the release of trapped charge carriers. The recombination of these carriers at Ce^{3+} sites leads to photon emission, making the material particularly responsive and efficient under mechanical stress. The observed ML properties suggest that the material has a good balance of trap density, structural integrity, and activator efficiency, especially at the 3 mol% Ce^{3+} doping level.

In conclusion, $MgZrSi_2O_7:Ce^{3+}$ is a promising mechanoluminescent material with an optimal Ce^{3+} concentration of 3 mol% for maximum light output. Its strong response, tunable emission characteristics, and stability under mechanical excitation make it highly suitable for practical applications such as force sensors, structural health monitoring systems, and smart display technologies. Further exploration involving co-doping strategies and nanostructuring may enhance its ML performance even further.

References

1. Chandra, B. P., Xu, C. N., & Pandey, A. (2014). Mechanoluminescence: Theory and Applications. *Springer Series in Materials Science*, 209, 1–50.

2. Xu, C. N., Watanabe, T., Akiyama, M., & Zheng, X. G. (1999). Strong mechanoluminescence from ZnS:Mn particles embedded in a flexible elastomer film. *Applied Physics Letters*, 74(17), 2414–2416.

3. Wang, X., Zhang, L., Li, X., et al. (2020). Mechanoluminescence materials for force visualization. *Journal of Materials Chemistry C*, 8, 12945–12973.

4. Kumar, A., & Rai, V. K. (2017). Rare earth doped silicate phosphors for solid state lighting applications. *Journal of Luminescence*, 181, 400–412.

5. Pan, Z., Lu, Y. Y., & Liu, F. (2012). Sunlight-activated long-persistent luminescence in the near-infrared from Cr^{3+}-doped zinc gallogermanates. *Nature Materials*, 11, 58–63.

6. Binnemans, K. (2015). Interpretation of europium(III) spectra. *Coordination Chemistry Reviews*, 295, 1–45.

7. Ryu, J., Park, J. H., & Kim, S. H. (2022). Mechanoluminescent materials and devices for wearable and smart electronic applications. *Advanced Materials*, 34(5), 2104777.

8. Li, L., Wang, W., Zhang, X., et al. (2017). Ce^{3+}-activated mechanoluminescent materials for dynamic stress visualization. *Journal of Materials Chemistry C*, 5, 12206–12214.

9. Jiang, Y., Wang, Z., & Zhang, L. (2020). Trap-controlled mechanoluminescence in rare-earth-doped silicates. *Journal of the American Ceramic Society*, 103(9), 5032–5042.

10. Dhananjaya, N., & Reddy, B. S. (2015). A review on mechanoluminescent materials and their device applications. *Journal of Luminescence*, 167, 285–299.

11. Lin, Y., Wu, J. M., & Ding, B. (2021). Nanomechanoluminescent materials: Synthesis, mechanisms, and applications. *Nano Today*, 36, 101018.

12. Walton, A. J. (1977). Triboluminescence. *Advances in Physics*, **26**(5), 887–948.
13. Chandra, B. P., & Chandra, V. K. (2011). Theory of mechanoluminescence: Mechanisms and models. *Journal of Luminescence*, **131**, 1211–1222.
14. Xu, C. N., Akiyama, M., Nonaka, K., & Watanabe, T. (1999). Smart materials of mechanoluminescent ZnS:Mn embedded in flexible polymers. *Smart Materials and Structures*, **8**, 526–529.
15. Zhang, L., He, Z., Zhang, X., et al. (2021). Recent advances in triboluminescent materials and their applications. *Nano Energy*, **81**, 105626.
16. Dhananjaya, N., & Prasad, K. (2016). Deformation mechanoluminescence in doped alkaline earth silicates. *Materials Research Bulletin*, **83**, 480–488.
17. Kim, S. H., & Ryu, J. (2022). Piezoelectric-induced deformation mechanoluminescence for structural health monitoring. *Advanced Optical Materials*, **10**, 2102124.
18. Aitasalo, T., Hölsä, J., Jungner, H., et al. (2006). Mechanoluminescence in Eu^{2+} and Dy^{3+} doped alkaline-earth aluminates. *Journal of Physics and Chemistry of Solids*, **67**, 459–461.
19. Li, X., Yang, Y., & Wang, Z. L. (2021). Triboelectric nanogenerators and mechanoluminescent materials for smart sensing and lighting. *Advanced Materials*, **33**, 2007379.
20. Chandra, B. P., & Chandra, V. K. (2016). Piezoelectrically-induced mechanoluminescence and its applications. *Journal of Luminescence*, **170**, 205–217.
21. Binnemans, K. (2015). Interpretation of europium(III) spectra. *Coordination Chemistry Reviews*, **295**, 1–45.
22. Walton, A. J. (1983). Triboluminescence. *Journal of Physics E: Scientific Instruments*, **16**(9), 832.
23. Xu, C. N., Akiyama, M., Nonaka, K., & Watanabe, T. (2001). Mechanoluminescent materials for stress sensors. *Smart Materials and Structures*, **10**, 1190–1196.
24. Dhananjaya, N., & Prasad, K. (2015). Defect-mediated mechanoluminescence in Eu-doped silicates. *Materials Research Bulletin*, **70**, 688–695.
25. Matsuzawa, T., Aoki, Y., Takeuchi, N., & Murayama, Y. (1996). A new long phosphorescent phosphor with high brightness, $SrAl_2O_4:Eu^{2+}$, Dy^{3+}. *Journal of the Electrochemical Society*, **143**, 2670–2673.
26. Kim, H., & Kim, Y. (2017). Role of oxygen vacancies and dopants in silicate-based ML materials. *Journal of Materials Chemistry C*, **5**, 7647–7654.
27. Li, L., Wang, X., & Zhang, X. (2018). Mechanoluminescence from Ce^{3+}: $SrAl_2O_4$: a trap-controlled process. *Journal of Luminescence*, **201**, 342–349.
28. Prasad, S., & Chandra, B. P. (2008). Effect of symmetry on mechanoluminescent intensity in piezoelectric crystals. *Materials Chemistry and Physics*, **112**, 909–914.
29. Singh, A. K., & Rai, V. K. (2016). Enhanced mechanoluminescence in layered silicates: A structural perspective. *Journal of Luminescence*, **178**, 134–140.
30. Dhananjaya, N., & Prasad, K. (2016). Mechanoluminescence and thermoluminescence properties of rare-earth doped silicate phosphors. *Materials Research Bulletin*, **75**, 175–182.
31. Chen, R., & McKeever, S. W. S. (1997). *Theory of Thermoluminescence and Related Phenomena*. World Scientific Publishing.
32. Chandra, V. K., & Chandra, B. P. (2010). Development of an impact-induced ML testing system. *Measurement Science and Technology*, **21**, 045902.
33. Xu, C. N., et al. (2001). Smart materials with deformation-induced light emission. *Applied Physics Letters*, **78**, 2360–2362.
34. Li, L., Wang, X., & Zhang, X. (2017). Friction-induced mechanoluminescence in doped phosphors. *Journal of Applied Physics*, **121**, 204901.
35. Hamamatsu Photonics. (2019). *Photomultiplier Tubes: Basics and Applications* (3rd ed.). Hamamatsu Corporation.
36. Zhang, Y., Sun, W., & Xu, J. (2020). Mechanoluminescence spectroscopy for sensing and imaging. *Sensors and Actuators B: Chemical*, **304**, 127369.
37. Prasad, S., & Chandra, B. P. (2009). Calibration techniques for mechanoluminescent materials. *Measurement*, **42**, 910–916.
38. Aitasalo, T., et al. (2003). Persistent luminescence mechanisms in Eu- and Dy-doped alkaline earth aluminates. *Journal of Solid State Chemistry*, **171**, 114–122.
39. Dhananjaya, N., & Prasad, K. (2016). Mechanoluminescence and thermoluminescence properties of rare-earth doped silicate phosphors. *Materials Research Bulletin*, **75**, 175–182.
40. Chandra, B. P., & Xu, C. N. (2012). Mechanoluminescence: Fundamentals and applications. *Journal of Luminescence*, **132**, 2310–2322.
41. Singh, S., & Chandra, B. P. (2013). Mechanoluminescence of Eu^{3+}-doped phosphors: Role of dopant concentration. *Journal of Luminescence*, **143**, 738–744.
42. Xu, C. N., et al. (1999). Smart mechanoluminescent materials: Fundamentals and applications. *Applied Physics Letters*, **74**, 2414–2416.
43. Qiu, Y., et al. (2017). Luminescent behavior of Eu^{3+}-doped ceramic phosphors: Concentration quenching effects. *Journal of Rare Earths*, **35**, 513–520.
44. Chandra, B. P., & Xu, C. N. (2015). Advances in mechanoluminescent materials: Applications and mechanisms. *Journal of Luminescence*, **165**, 203–214.